energies

MDPI

Article

System-Level Modeling and Thermal Simulations of Large Battery Packs for Electric Trucks

Anandh Ramesh Babu [1,*], Jelena Andric [1], Blago Minovski [2] and Simone Sebben [1]

[1] Division of Vehicle Engineering and Autonomous Systems, Chalmers University of Technology, Chalmersplatsen 4, 412 96 Göteborg, Sweden; jelena.andric@chalmers.se (J.A.); simone.sebben@chalmers.se (S.S.)
[2] Volvo Technology AB, Götaverksgatan 10, 417 55 Göteborg, Sweden; blago.minovski@volvo.com
* Correspondence: anandh.rameshbabu@chalmers.se; Tel.: +46-734917178

Abstract: Electromobility has gained significance over recent years and the requirements on the performance and efficiency of electric vehicles are growing. Lithium-ion batteries are the primary source of energy in electric vehicles and their performance is highly dependent on the operating temperature. There is a compelling need to create a robust modeling framework to drive the design of vehicle batteries in the ever-competitive market. This paper presents a system-level modeling methodology for thermal simulations of large battery packs for electric trucks under real-world operating conditions. The battery pack was developed in GT-SUITE, where module-to-module discretization was performed to study the thermal behavior and temperature distribution within the pack. The heat generated from each module was estimated using Bernardi's expression and the pack model was calibrated for thermal interface material properties under a heat-up test. The model evaluation was performed for four charging/discharging and cooling scenarios typical for truck operations. The results show that the model accurately predicts the average pack temperature, the outlet coolant temperature and the state of charge of the battery pack. The methodology developed can be integrated with the powertrain and passenger cabin cooling systems to study complete vehicle thermal management and/or analyze different battery design choices.

Keywords: lithium-ion battery; battery pack modeling; module discretized thermal simulation; electric truck

check for updates

Citation: Ramesh Babu, A.; Andric, J.; Minovski, B.; Sebben, S. System-Level Modeling and Thermal Simulations of Large Battery Packs for Electric Trucks. *Energies* **2021**, *14*, 4796. https://doi.org/10.3390/en14164796

Academic Editor: Carlos Miguel Costa

Received: 9 July 2021
Accepted: 2 August 2021
Published: 6 August 2021

Publisher's Note: MDPI stays neutral with regard to jurisdictional claims in published maps and institutional affiliations.

Copyright: © 2021 by the authors. Licensee MDPI, Basel, Switzerland. This article is an open access article distributed under the terms and conditions of the Creative Commons Attribution (CC BY) license (https://creativecommons.org/licenses/by/4.0/).

1. Introduction

With global demand for energy resources increasing due to economic growth, the risk of energy crisis and environmental pollution is on the rise as the majority of energy for the transport sector is still derived from fossil fuels [1,2]. Over the last decade, the automobile industry has been intensifying its efforts towards battery electric vehicles (BEVs) to comply with new regulations and the public awareness to combat the negative effects of climate change. The emission cap for road vehicles has decreased with each new regulation and this limit is expected to reduce even further in the coming years [3]. The development of Lithium-ion (Li-ion) batteries has made it possible for BEVs to emerge as a promising means of transportation where the electricity from them is used to power the vehicle instead of fossil fuels. BEVs also have low operational costs, high performance and are efficient, which helps gratify the stakeholders and propel the technology into the market [4].

Large battery packs are required for vehicle applications to meet the high power demand. A battery pack is a complex system consisting of a number of battery modules (which contain cells that are connected in series and parallel), battery management system and cooling/heating circuits. For BEVs, battery packs not only provide energy to power the propulsion system, but also acclimatize the entire powertrain and the passenger compartment. Therefore, the performance of the battery pack is crucial to the operation, reliability and safety of the vehicle.

Batteries are electrochemical systems and their performance is highly dependent on the thermal operating environment. During the battery pack operations, heat is generated by the battery cells and other electronic components due to current flow and internal resistances. However, temperature levels and uniformity significantly influence the performance, safety and lifespan of the battery [5]. At high temperatures, the cells experience high impedance, accelerated ageing or even thermal runaway [6,7]. At low temperatures, their efficiency drops considerably, leaving the discharge capacity minimal [8–10]. This effect is important to address since, in cold climates, a large portion of the energy from the battery is spent on heating itself and the cabin, thus shortening the driving range by more than 30–40% [11,12]. Moreover, non-uniform temperature distribution within the pack leads to unbalanced charging/discharging in modules, thereby reducing the performance utilization of the pack. It is therefore important to maintain the optimum operating temperature range for all the modules and minimize module-to-module temperature variations. Hence, efficient battery thermal management strategies (BTMSs) to improve the thermal efficiency of batteries are crucial.

Battery heat generation is a complex phenomenon which requires knowledge from different disciplines to understand the governing physics behind it. There exist several categories of battery models that can predict battery behavior with different levels of accuracy. The two most common categories are the electrochemical and equivalent circuit models. The electrochemical models are typically employed to describe the electrochemical reactions, transport phenomena and heat dissipation at the cell level [13,14]. While being the most detailed and accurate, they are time-consuming and hence not suitable for the analysis of BTMS in large battery packs. Equivalent circuit models, which use empirical equations modeled using experimental data, perform well for highly dynamic simulations and run faster than electrochemical models [15].

A good deal of modeling and simulation studies have been conducted to predict and analyze the thermal behavior of battery packs. Several studies employed the three dimensional (3D) computational fluid dynamics (CFD) approach for studying the thermal behavior of battery modules and packs. Wang et al. [16] presented an overview of the vast theoretical research on 3D modeling of batteries. Basu et al. proposed a novel temperature correlation based on a coupled electrochemical 3D CFD model, which can predict the temperature of all the cells in a battery pack based on the measurement of one cell temperature [17]. Saqli et al. [18] presented the modeling methodology of a one-dimensional (1D) electrochemical model coupled with 3D CFD approach to study the thermal behavior of cylindrical cells and later built a thermal first-order equivalent circuit model. Various parametric studies in 3D have been used to improve the designs of cooling strategies and understand the effect operating conditions have on the behavior of different thermal management systems [19–21]. While 3D simulations are very accurate and provide a high level of detail, they are extremely time-consuming and require a lot of computational resources. System level modeling approach, on the other hand, is a fast and useful technique to analyze a battery's thermal behavior as compared to the 3D approach. Alhanouti et al., in [22], proposed a new model to accurately estimate the reversible part of heat generated in Bernardi's model [23]. A lumped thermal model was implemented to simulate the development of temperature in a cell and later extended it to a pack. Gao et al., in [24], used an equivalent circuit model in combination with a convective thermal model to estimate the electrical parameters and the temperature of the cells in a 12-cell battery pack. Gottapu et al. [25] proposed a simplified electrochemical model and lumped thermal model to analyze the thermal distribution at the pack level. Shabani et al., in [26], presented an overview of the different theoretical, numerical and analytical approaches to thermal modeling in batteries. Recently, Astaneh et al. [27] presented a novel module-to-module discretized modeling framework that employs electrochemical-thermally coupled battery model. The proposed framework makes it possible to capture the temperature non-uniformities with the purpose of performing studies that couple the cell properties to the pack's performance. The main challenges with battery modeling still remain when it

comes to finding the trade-off between model complexity and fidelity on one side and the computational speed on the other side to facilitate dynamic simulations at the pack level and capture subsystem interaction at the vehicle level. The development of a comprehensive simulation framework that makes it possible to understand and predict the behavior of the battery pack and integrate it at the vehicle level is essential.

This work is a step towards developing such a vehicle-level simulation framework. The study presents a modeling methodology for battery pack thermal simulations for an electric truck under realistic operating conditions. A system-level modeling approach was used to model the battery pack in GT-SUITE. Navier–Stokes equations in 1D and analytical correlations were employed to capture the flow and heat transfer in the battery pack, respectively. The battery pack was discretized at the module level and the heat generated by each module was estimated using Bernardi's model [23]. The experimental data from physical tests performed on the battery pack were used for model calibration and validation. Dynamic current profiles and coolant inlet characteristics were chosen to ensure the robustness of the model.

This paper is organized as follows: Section 2 describes the battery pack modeling framework, outlining the pack configuration and the theoretical background for computing the fluid and heat flow. Section 3 presents the battery pack simulation methodology comprising the model calibration to the experimental data and four representative test case scenarios for model validation. Section 4 depicts the findings of the study by comparing the simulation results with the experiments.

2. Battery Pack Modeling Framework

The geometry of the battery pack and its cooling system together with the analytical and numerical methods used to describe and solve the underlying physics of the problem are described in this section.

2.1. Battery Pack Configuration

The geometries of the battery pack and the cooling system are shown in Figure 1a. The battery system has a 180s2p configuration (where s stands for series and p stands for parallel) and uses indirect liquid cooling strategy. The pack consists of two trays, placed one on top of the other. Each tray includes battery modules, an aluminium cooling plate and thermal interface material between the module casings and the cooling plate as shown in Figure 1b. Each module has several prismatic NMC-111 type Li-ion cells. The cooling plates have two common railings, one connected to the inlet and the other connected to the outlet. The railings are connected to rows of U-shaped channels. Every row consists of three micro-channels that are used to cool the modules. The whole setup is enclosed in a stainless steel casing (not shown in the figure).

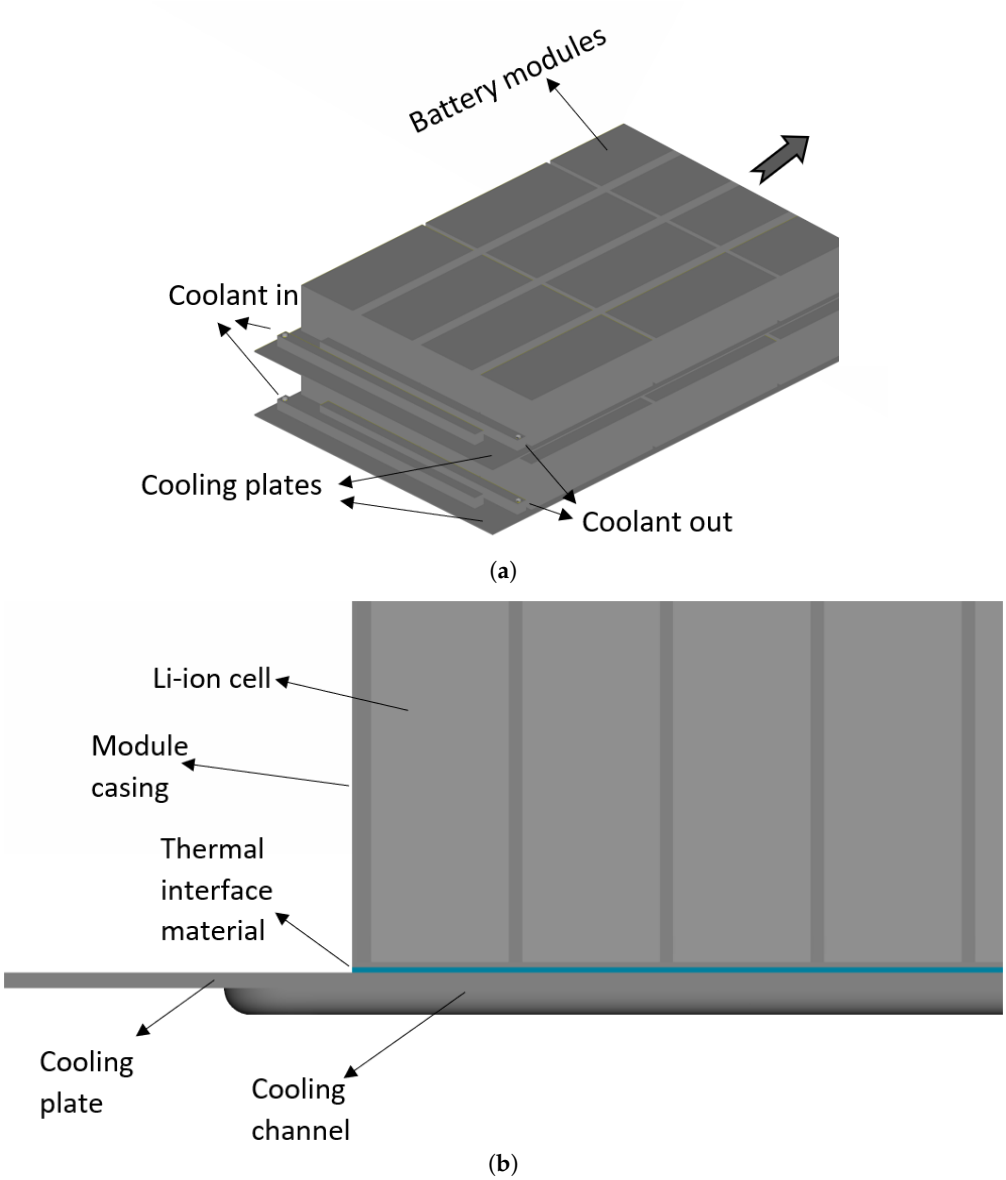


Figure 1. 3D representation of the battery pack: (**a**) isometric view; (**b**) Cross-sectional view of the module assembly.

2.2. Flow and Energy Modeling

Each coolant microchannel was discretized into seven tubes that the coolant, a 40–60 mixture of glycol-water, flows through. The incompressible conservation equations, namely continuity, momentum and energy as seen in Equations (1)–(3), respectively, were solved numerically to compute the fluid and heat flow in the model:

$$\text{Continuity equation: } \nabla \cdot \vec{U} = 0 \tag{1}$$

$$\text{Momentum equation: } \rho \frac{D\vec{U}}{Dt} = \nabla P + \nabla \cdot (\mu \nabla \vec{U}) \tag{2}$$

$$\text{Energy equation: } \rho c_p \frac{DT}{Dt} = \nabla \cdot (k \nabla T) \tag{3}$$

where $\vec{U}$ is the velocity of the fluid, ρ is the density of the fluid, $\frac{D}{Dt}$ is the total derivative of the quantity ($\frac{D}{Dt} = \frac{\partial}{\partial t} + (\vec{U} \cdot \nabla)$), ∇P is the pressure gradient, μ is the dynamic viscosity, c_p is the specific heat capacity of the fluid, T is the temperature and k is the thermal conductivity of the fluid.

The conservation equations were discretized using the control volume method on a staggered grid. The transient simulations were solved implicitly with a timestep size of 0.1 s.

The scalar and vector quantities are solved only in the direction of fluid flow. In order to couple the heat transfer between the fluid and solids, the heat transfer coefficient (h) must be estimated. Since the boundary layer is not resolved in the wall normal direction, the heat transfer coefficient between the wall of the cooling channel and the coolant was calculated using an analytical heat transfer correlation for internal convection. It is worth mentioning that several analytical correlations available in GT-SUITE were tested and they all produced very similar results. Colburn analogy [28], as seen in Equation (4), was chosen due to its wide usage and straightforward implementation:

$$j_{th} = \frac{Nu_D}{Re_D Pr^{1/3}} \tag{4}$$

where j_{th} is the j-factor, Nu_D and Re_D are the Nusselt and Reynold's numbers, respectively, based on the channel's diameter and Pr is the Prandtl number. Reynold's number reads:

$$Re_D = \frac{UD}{\nu} \tag{5}$$

where $\nu = \mu/\rho$ is the kinematic viscosity of the fluid.

The Prandtl number is the ratio of the kinematic viscosity and the thermal diffusivity ($\alpha = \frac{k}{\rho c_p}$):

$$Pr = \frac{\nu}{\alpha} \tag{6}$$

and the Nusselt number is calculated as:

$$Nu_D = \frac{hD}{k} \tag{7}$$

For pipe flows, the values of j_{th} are typically around $C_f/2$ [29], where C_f is the Fanning friction factor and defined for laminar flows ($Re_D < 2000$) [28] as:

$$C_f = \frac{16}{Re_D} \tag{8}$$

Hence, after computing Reynold's number for the cooling channel, the j-factor and the heat transfer coefficient were estimated. It should be noted that the usage of the Colburn analogy relies on the assumption that the flow is fully developed both hydrodynamically and thermally throughout the microchannels. This means that the variations of the heat transfer coefficient in the entrance region were not captured in the model. The influence of this assumption is further discussed in Section 4.2.

The heat transferred (Q) between the coolant and the cooling plate was then computed as:

$$Q = hA(T_w - T_f) \tag{9}$$

where A is the surface contact area between the cooling plate wall and the coolant, T_w is the surface temperature of the cooling plate and T_f is the bulk coolant temperature.

The coolant's volumetric flow rate and temperature were imposed at the inlet. The pressure at the outlet was set to match the measured data. The Neumann boundary condition was applied for the fluid temperature at the outlet.

The battery pack was discretized at the module level. Each battery module was represented as a single thermal mass. The consequence is that all cells in the battery module have the same temperature. This assumption holds for relatively low C-rates when the cell temperatures are approximately constant.

The battery modules were in contact with the module casing and heat transfer between the two was modeled through conduction. Each cooling plate was discretized into 20 lumped thermal masses and they were thermally connected with each other to account for conduction. The temperature of each lumped mass at any instant is calculated using the expression:

$$\dot{Q}_{net} = mc_p \frac{dT}{dt} \tag{10}$$

where $\dot{Q}_{net}$ is the net rate of heat accumulation in the lumped mass, m is its mass, c_p is the specific capacity of the material and $\frac{dT}{dt}$ is the rate of change in temperature of the lumped mass.

The thermal interface material present between the module casing and the cooling plate was modeled using a thermal resistance where the thickness and the thermal conductivity of the interface material, which are unknowns, can be represented as one variable. The thermal resistance of the interface to the transfer of heat is then given by:

$$R_{th} = \frac{t_{TIM}}{kA_c} \tag{11}$$

where t_{TIM} is the thickness of the thermal interface material, k is its thermal conductivity and A_c is the area of contact.

Finally, the battery casing, made of stainless steel, was modeled as a separate thermal mass. The heat transfer between the battery casing and the environment was established using a heat transfer coefficient and based on analytical correlations and CFD simulations, it was estimated to 2.6 W/m^2K. Table 1 shows the properties of the materials used in the battery pack.

Table 1. Physical properties of the materials in the battery pack used in the model.

Material	Aluminium	Stainless Steel	Coolant	Li-ion Battery
Density (kg/m^3)	2702	7900	1057	1827
Thermal conductivity (W/mK)	237	14.9	0.423	19.3
Specific heat (J/kgK)	903	477	3484	1145
Dynamic viscocity (Pa/s)	-	-	0.0023	-

2.3. Battery Module Modeling

Bernardi's model of heat generation [23] was used to estimate the heat generated from each module which reads:

$$\dot{Q} = N_{mod}\left(I^2 R_{int} + IT\left(\frac{dU_{ocv}}{dT}\right)\right) \tag{12}$$

where $\dot{Q}$ is the heat generated, N_{mod} is the number of cells in a module, I is the current, R_{int} is the internal resistance of the cells in the module, T is the temperature of the battery module and $\frac{dU_{ocv}}{dT}$ is the entropic coefficient. R_{int} and $\frac{dU_{ocv}}{dT}$ were obtained based on measurements performed on the battery pack.

The first term on the right hand side of Equation (12) is the heat generated due to irreversible ohmic loss and the second term on the right hand side is due to reversible entropic heat loss. R_{int} is a function of the temperature of the module and its state of charge (SoC), and $\frac{dU_{ocv}}{dT}$ is a function of SoC. These quantities were interpolated accordingly during the simulation. The SoC of the battery pack was estimated in the model as:

$$SoC = SoC_0 + \frac{1}{C}\int_0^t \eta_b I dt \tag{13}$$

where SoC_0 is the initial SoC, C is the capacity of the battery and η_b is the efficiency of the battery.

3. Simulation Methodology

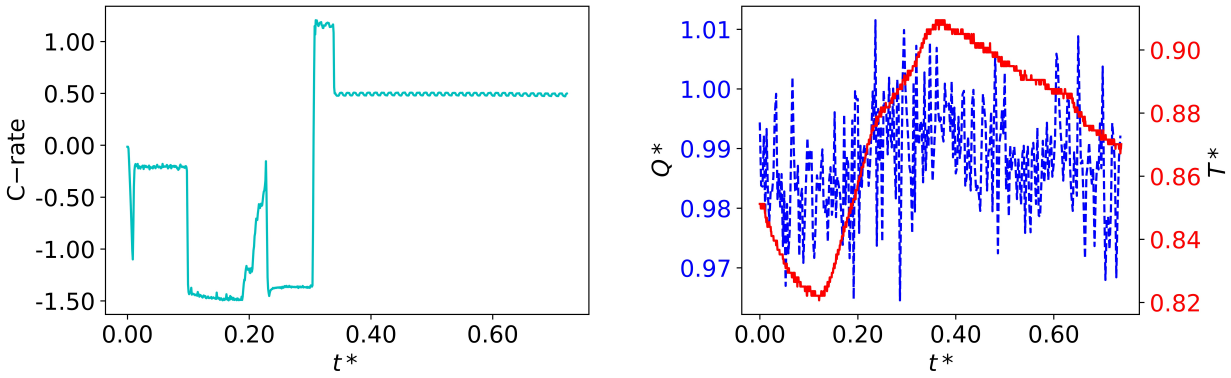
3.1. Model Calibration Optimization

The resistance of the thermal interface material is often an unknown quantity while modeling a battery pack as this information is withheld by the battery supplier. For this reason, data from the heat-up test of the battery pack were used to estimate its value. The battery pack with the initial temperature of $0.233T^*$ (where $T^* = T/T_{ref}$ and T_{ref} is a randomly chosen reference temperature) was heated by the coolant at $0.833T^*$ flowing at $0.8\ Q^*$ (where $Q^* = Q/Q_{ref}$ and Q_{ref} is a randomly chosen reference volume flow rate) and the average pack temperature was measured. The battery pack was inactive and so there was no heat generated from it. The thermal resistance was optimized in the model using the Nelder–Mead optimization approach [30] with the objective to minimize the difference between the experimental and simulation values for the average pack temperature.

3.2. Case Studies for Model Validation

The developed battery pack model was validated using the experimental data from four test scenarios herein referred to as Cases 1–4. The test scenarios depict the typical real-world operating conditions for large battery packs in electric trucks.

Case 1 represents a discharging/charging cycle. Figure 2 illustrates the pack operation under the scenario of Case 1. The transient current profile (Figure 2a) shows that the C-rates were varied between −1.5 and 1 C followed by a constant current charging at 0.5 C. The volumetric flow of the coolant was kept nearly constant at the inlet and a small variation in its temperature was observed as shown in Figure 2b.



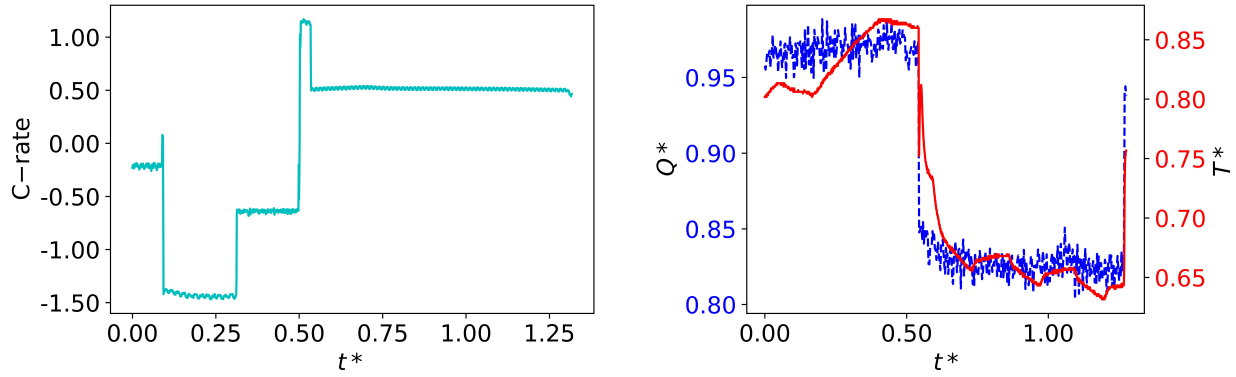
(**a**) (**b**)

Figure 2. Case 1 test scenario: (**a**) Current profile —— and (**b**) inlet volumetric flow rate (Q^*) - - - - and temperature of the coolant (T^*) ——.

Case 2 represents a similar discharging/charging profile as Case 1 (Figure 3a) with the addition of a both coolant volumetric flow rate and temperature being varied at the inlet of the battery pack as seen in Figure 3b. These variations were achieved by reducing the power of the coolant pump in the cooling system and increasing the power of the fan for the radiator cooling.

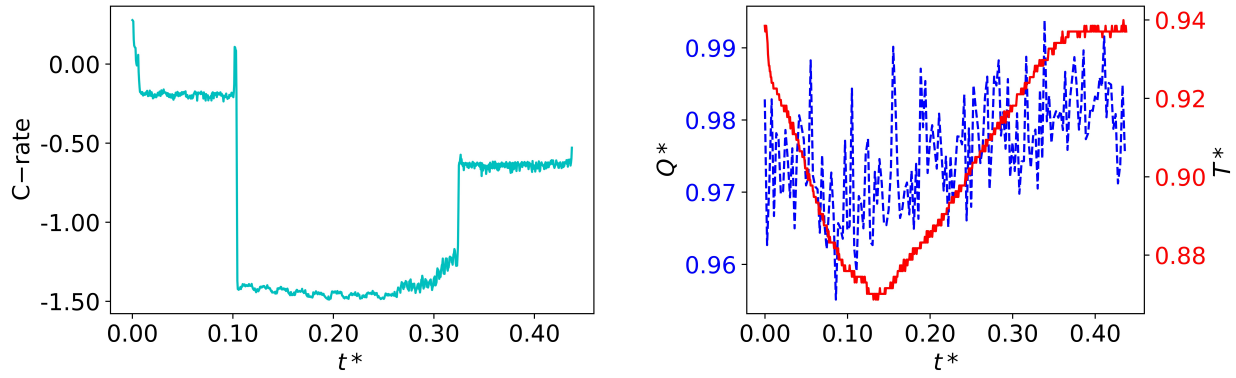
Case 3 is a discharge cycle with three approximately constant current rates (−0.25, −1.5 and −0.75 C) as displayed in Figure 4a. The coolant volumetric flow rate and its temperature at the inlet were maintained nearly constant (Figure 4b).

Finally, Case 4 depicts a cooling scenario when the battery pack is not operating (Figure 5a). Here, the coolant flow rate at the inlet was decreased gradually throughout the cycle by decreasing the power of the pump, as the temperature of the battery pack decreased. This is reflected in the coolant's temperature at the inlet as well, see Figure 5b.



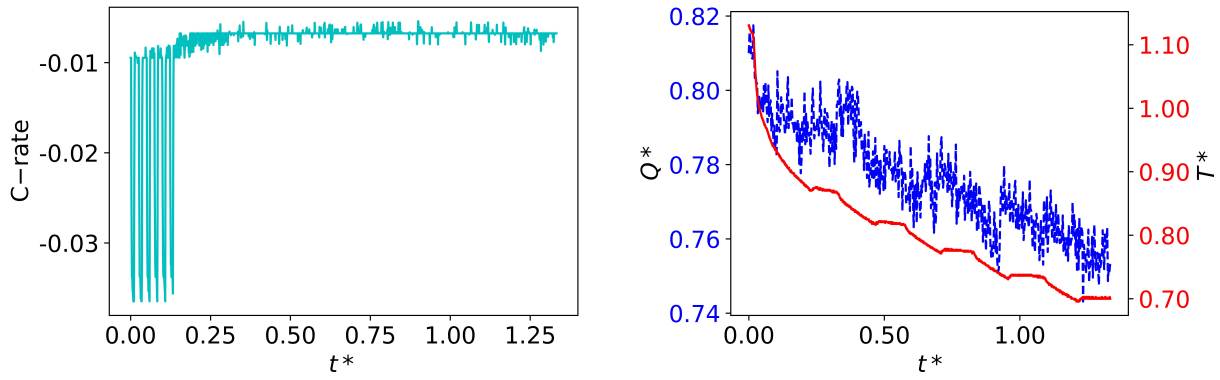
(**a**) (**b**)

Figure 3. Case 2 test scenario: (**a**) Current profile —— and (**b**) inlet volumetric flow rate (Q^*) - - - - and temperature of the coolant (T^*) ——.



(**a**) (**b**)

Figure 4. Case 3 test scenario: (**a**) Current profile —— and (**b**) inlet volumetric flow rate (Q^*) - - - - and temperature of the coolant (T^*) ——.



(**a**) (**b**)

Figure 5. Case 4 test scenario: (**a**) Current profile —— and (**b**) inlet volumetric flow rate (Q^*) - - - - and temperature of the coolant (T^*) ——.

4. Results and Discussion

4.1. Battery Pack Model Calibration

First, the battery pack model was calibrated using experimental data for the average pack temperature during the heat-up test. The objective was to minimize the difference between the experimental and the simulation results for the average temperature of the

battery pack by varying the thermal resistance of the thermal interface material between the cooling plates and the battery modules. Figure 6 shows the comparison between measured and simulated temperature profiles for the heat-up test. The calibration yielded a thermal resistance of 0.004252 m^2K/W.

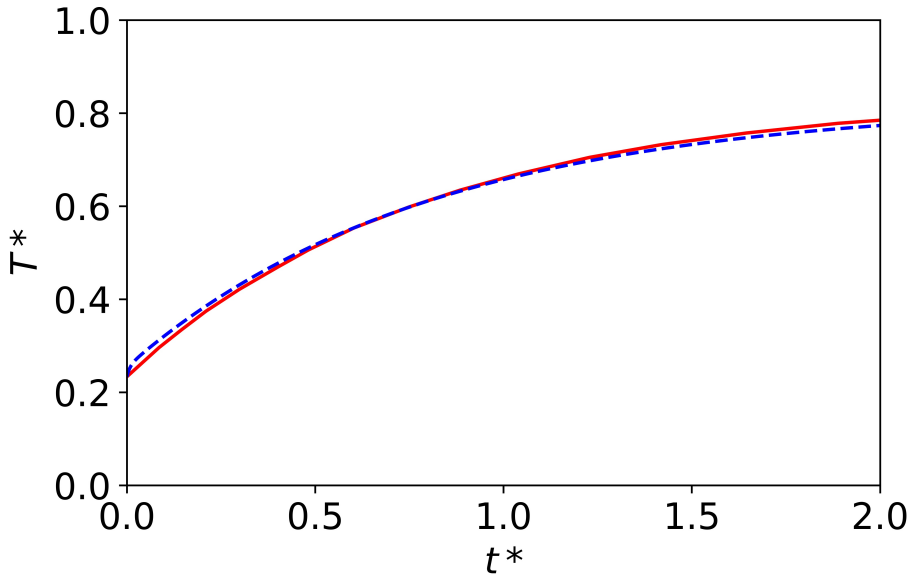


Figure 6. Average battery pack temperature during the heat-up test: Measured ——— ; simulated - - - -.

4.2. Case Studies for Model Validation

The battery pack model was validated using the experimental data for the average pack temperature, the outlet temperature of the coolant and the average SoC of the pack for four scenarios (Case 1–4) as described in Section 3.2. The validation results for Case 1 are presented in Figure 7.

It should be noted that the step profile in the experimental temperature values is due to the resolution of the sensors used during the measurements. The sensors used for the measurement of the average pack temperature were provided by the battery suppliers and hence could not be accessed or modified. Nonetheless, the average temperature of the battery pack predicted by the simulations is in good agreement with the measurements. The average battery pack temperature was predicted well both during discharging ($t^* < 0.3$) and charging ($t^* > 0.4$) but slightly underpredicted during the transition from discharging at -1.5 C to charging at 1 C ($0.3 < t^* < 0.4$). The temperature of the coolant at the outlet and the average SoC of the battery pack were estimated well from the simulation.

For Case 2, the simulated average temperature of the battery pack, displayed in Figure 8, was marginally overestimated compared to the measurements during the discharge phase ($t^* < 0.5$) with the maximum C-rate of -1.5 C, and underestimated during the charging phase most of which was at 0.5 C, with lower coolant volumetric flow rate and temperature. The outlet temperature of the coolant was slightly overpredicted from $t^* = 0.75$ until the end of the cycle. The average SoC for the battery pack was in very good agreement with the measurements through the entire cycle.

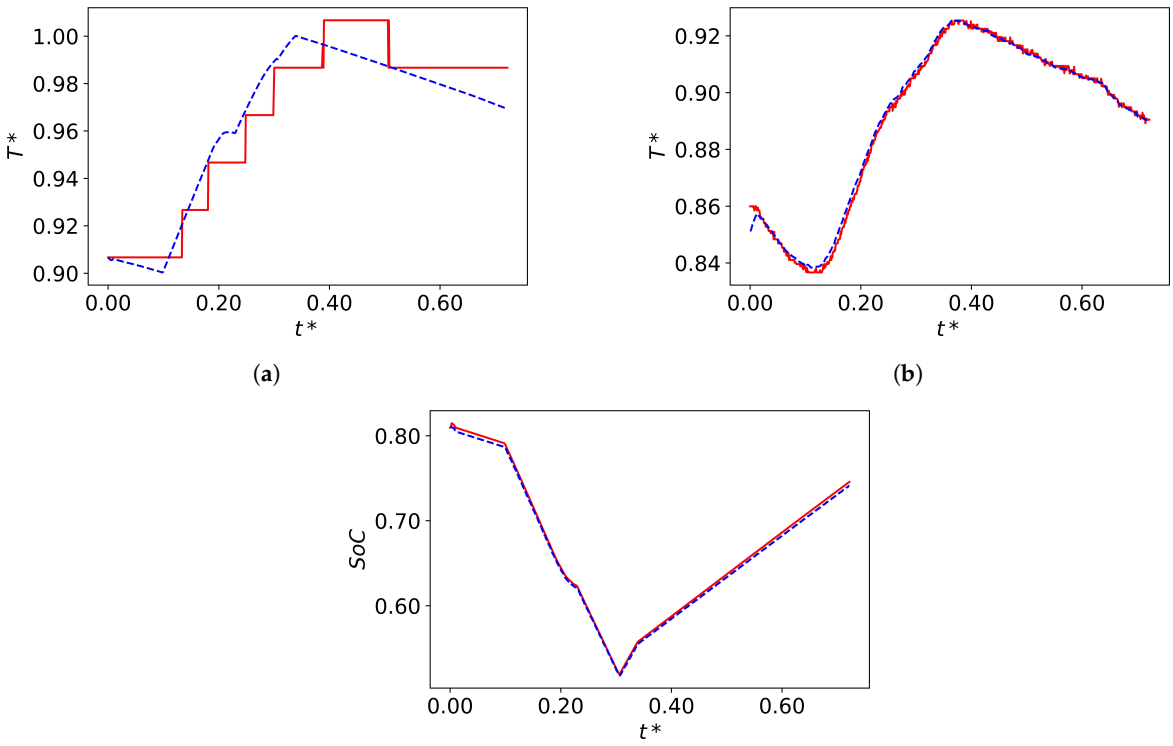


Figure 7. Results for Case 1: (**a**) average battery pack temperature, (**b**) outlet coolant temperature and (**c**) average battery pack SoC . Measured quantity ——— ; simulated quantity - - - -.

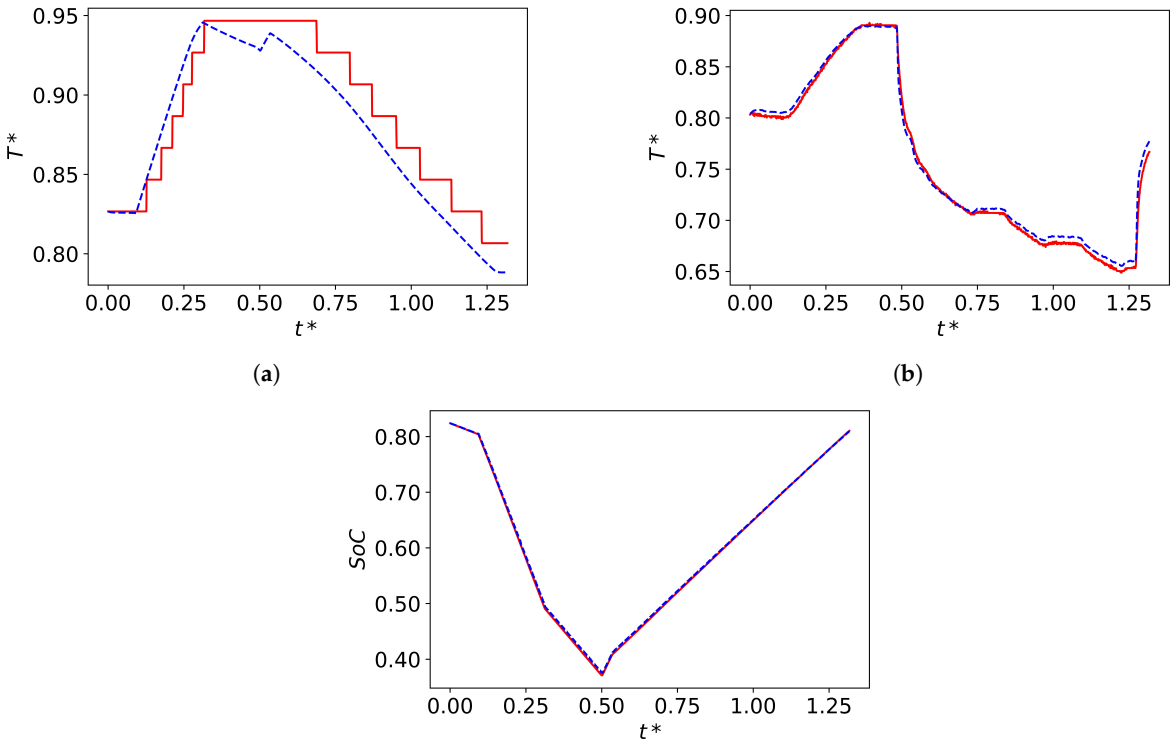


Figure 8. Results for Case 2: (**a**) average battery pack temperature, (**b**) outlet coolant temperature and (**c**) average battery pack SoC. Measured quantity ——— ; simulated quantity - - - -.

The results for Case 3, which consists of three discrete discharge profiles, are seen in Figure 9. The average temperature of the battery pack from the measurement and simulation agreed well with each other. The outlet temperature of the coolant and the average *SoC* were also estimated with very good accuracy.

The results for Case 4 that represents cool down of the battery pack with continuously decreasing coolant volumetric flow rate are shown in Figure 10. The variations in the average pack temperature are due to heat rejection from the pack to the coolant. The average temperature of the battery pack and the outlet temperature of the coolant were marginally overpredicted in the simulations as compared to the measurements.

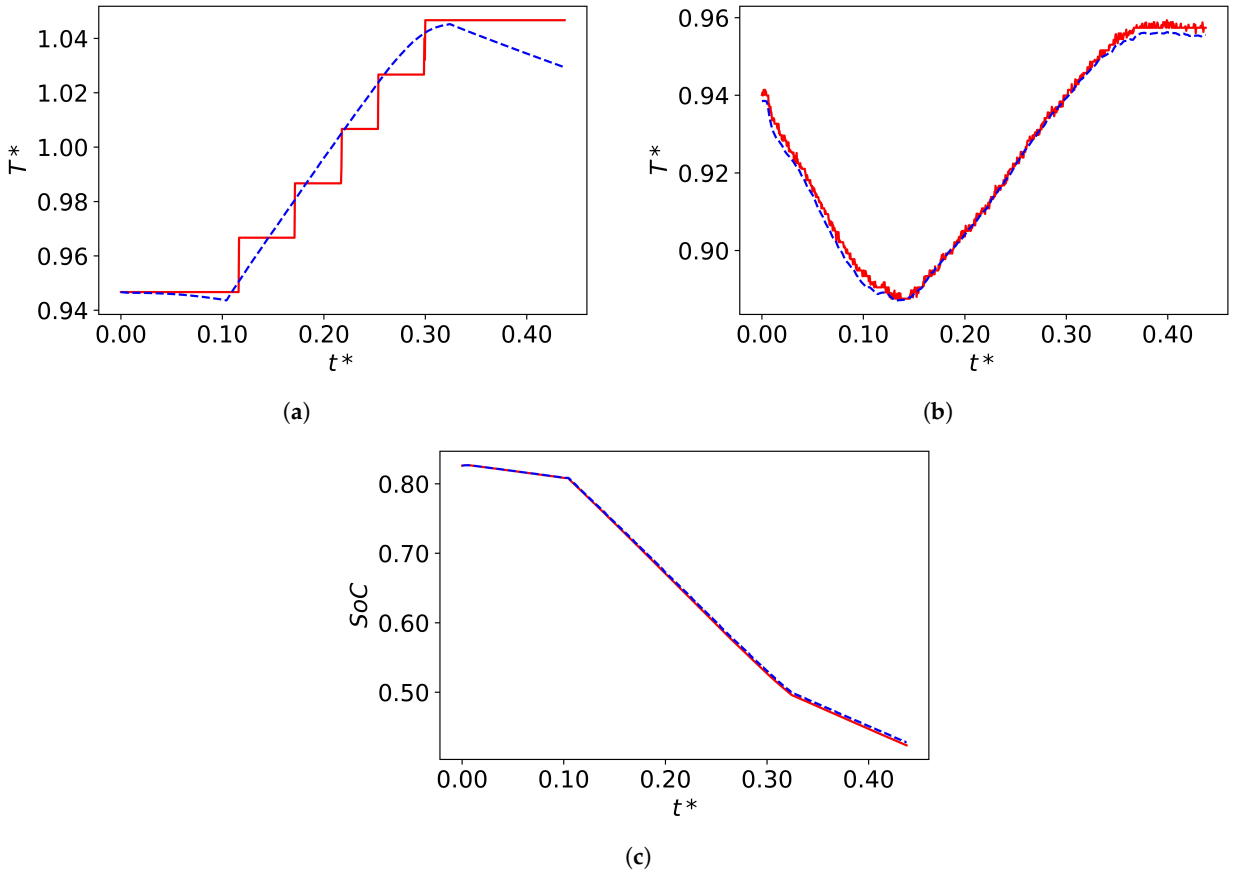


Figure 9. Results for Case 3: (**a**) average battery pack temperature, (**b**) outlet coolant temperature and (**c**) average battery pack SoC. Measured quantity ——; simulated quantity - - - -.

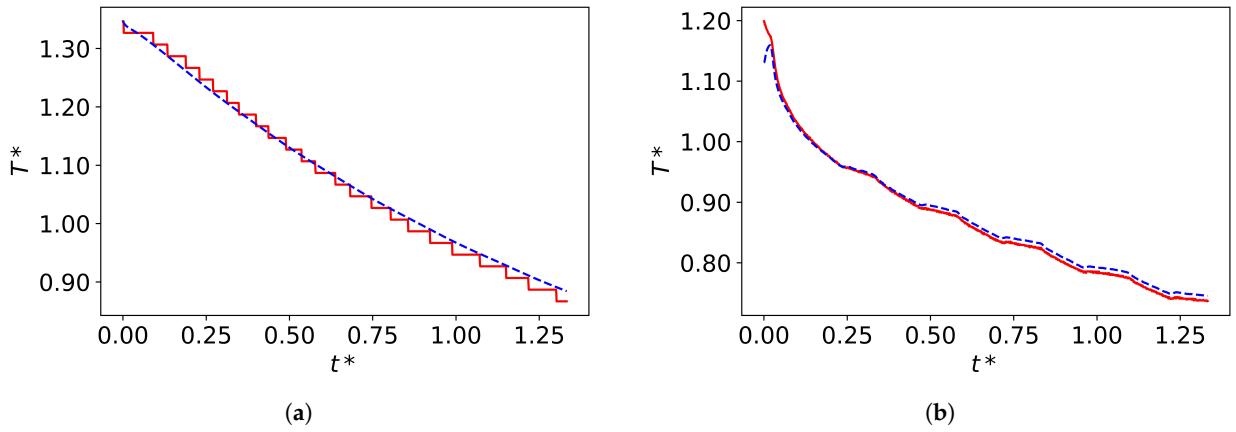


Figure 10. Results for Case 4: (**a**) average battery pack temperature and (**b**) outlet coolant temperature. Measured quantity ——; simulated quantity - - - -.

The root mean square (RMS) errors in the estimation of the average battery pack temperature, the outlet coolant temperature and the *SoC* of the battery pack are presented in Table 2. As it was seen from the plots, the error in estimation was slightly higher when the current profile and/or flow rate varied. Nevertheless, the magnitude of error is very low and in the order of the resolution of the sensors used.

Table 2. RMS errors between simulated and measured quantities for the four cases.

Case	Average Battery Pack Temperature (K)	Outlet Coolant Temperature (K)	SoC (%)
1	0.3291	0.0486	0.338
2	0.5474	0.1708	0.284
3	0.2405	0.0508	0.270
4	0.3576	0.2561	-

The transient profiles of the battery pack temperatures and the coolant outlet temperatures were estimated very well for Cases 1 and 3 with nearly steady conditions for coolant flow. Minor discrepancies were, however, observed for Cases 2 and 4 with dynamic coolant flow rates and temperature. These deviations can be attributed to the usage of empirical models for heat generation in the battery and heat transfer between the coolant and the wall. While these empirical models perform well in steady-state operating conditions, small deviations arise when the conditions are dynamic.

With the hydrodynamic entrance length around 1% of the total length of the microchannel, the flow is considered hydrodynamically fully developed. The thermal entrance length was estimated to be around 19% the total length of the microchannel. Nonetheless, the Colburn analogy was applied to the entire microchannel primarily due to current limitations in the software. While this is a shortcoming in the model, this simplification has a negligible effect on capturing the thermal behavior of the battery pack, as seen from the simulated and experimental results. The modeling framework relies on simplifying the physics to capture the important underlying features of the battery pack system.

The main advantage of discretizing the battery pack to the module level is that the temperature non-uniformity in the battery pack can be studied and monitored. The evolution of the maximum and minimum temperatures of the modules are plotted in Figure 11 for the four cases. They follow the same profiles as the average pack temperatures for the respective scenarios. The difference between the maximum and minimum temperatures between the modules ($dT^* = dT/dT_{ref}$, where dT_{ref} = 1/60 T_{ref}) is also shown. The temperature variations of the battery modules are due to differences in the rate of heat accumulated leading to different rates of temperature change during the pack operation. In the discharging/charging scenarios (Cases 1–3), dT^* changes at varying rates due to variations in the heat generated by the modules and the coolant flow characteristics. In Case 1, the increase in dT^* slowed down when the pack shifted from transient discharging to constant low current charging as the coolant flow was kept nearly constant. The difference dT^* increased at a higher rate in Case 2 due to the decrease in the coolant flow rate when shifting to constant charge. In Case 3, dT^* increased faster at the discharge current 1.5 C compared to lower discharge currents while the coolant flow characteristics were maintained constant throughout the test. In the cooling scenario (Case 4), however, dT^* increased logarithmically meaning that some modules were cooled better than others, leading to a rapid increase in temperature difference at the beginning before it reaches a plateau.

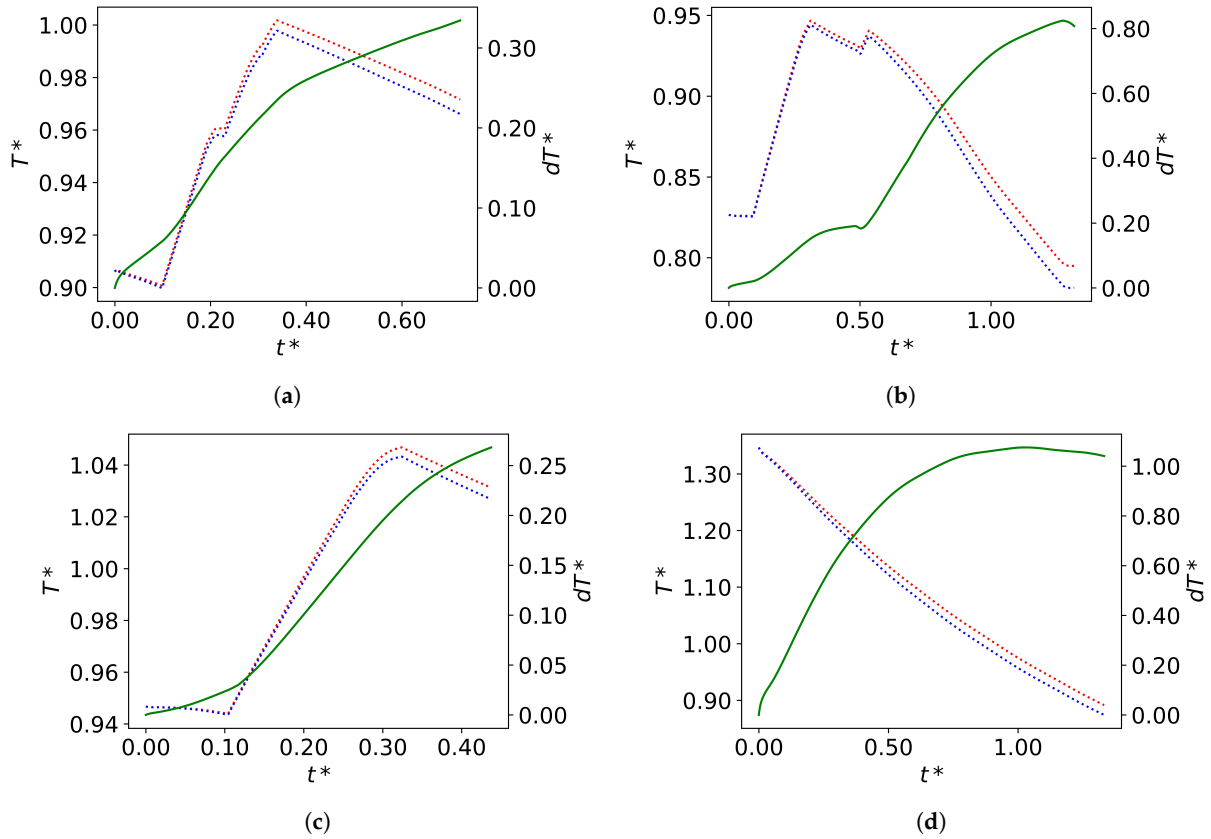


Figure 11. Variation in the maximum, minimum temperatures of the modules and their difference for each case: (**a**) Case 1, (**b**) Case 2, (**c**) Case 3 and (**d**) Case 4; T^*_{max} ----- , T^*_{min} ——— , dT^* ———.

5. Conclusions

This work focused on developing the modeling methodology based on 1D system-level approach to perform thermal simulations of large battery packs for electric truck applications. The battery pack consisted of two trays, each comprising a cooling plate, thermal interface material and Li-ion cells enclosed in a module casing. The pack was discretized at the module level and the heat generated from each module was estimated using Bernardi's model. One-dimensional (1D) formulation of the Navier–Stokes equations was used to solve the transport of flow and heat. An analytical Colburn correlation was used to predict the heat transfer coefficient between the cooling channels and coolant.

The thermal resistance of the thermal interface material between the modules and the cooling plates was used to calibrate the heat transfer between the battery modules and the coolant. The objective was to minimize the difference between the measured and simulated values for the pack average temperature during the heat-up test. The model was validated using four test scenarios representing battery pack charging/discharging during truck driving, as well as pack cooling after the truck was parked. The average temperature of the battery pack, the outlet temperature of the coolant and the SoC of the battery pack were estimated for each of these scenarios. The simulation results were in good agreement with the experimental data with RMS error less than 0.55 K when estimating the battery pack temperature, less than 0.26 K when estimating the outlet coolant temperature and less than 0.4% in the estimation of the SoC of the pack.

The results demonstrate the feasibility of the developed model for studying the thermal behavior of battery packs. The 1D modeling approach developed herein provides a trade-off between accuracy and speed, making it possible to expand the model for studying complete vehicle thermal management. Moreover, the model can be utilized to perform design studies to further improve the efficiency of the cooling strategy.

Finally, the work presented herein is highly relevant for different actors within electric vehicle system modeling, comprising automobile industries, battery manufacturers and other OEMs, as well as simulation software companies.

Author Contributions: Conceptualization, A.R.B., J.A., B.M. and S.S.; methodology, A.R.B.; software, A.R.B., B.M. and J.A.; validation, A.R.B.; formal analysis, A.R.B. and J.A.; investigation, A.R.; resources, B.M. and S.S.; data curation, A.R.B.; writing—original draft preparation, A.R.B.; writing—review and editing, A.R.B., J.A., S.S. and B.M.; visualization, A.R.B.; supervision, J.A. and B.M.; project administration, S.S.; funding acquisition, S.S. All authors have read and agreed to the published version of the manuscript.

Funding: This research was funded by the Swedish Energy Authority/FFI project number, D. nr P48024-1.

Institutional Review Board Statement: Not applicable.

Informed Consent Statement: Not applicable.

Data Availability Statement: Not applicable.

Acknowledgments: The authors would like to thank Majid Astaneh, Chalmers University of Technology and Masih Khoshab, Volvo Group Truck Technology for their valuable contributions to this work.

Conflicts of Interest: The authors declare no conflict of interest.

References

1. Dudley, B. BP Statistical Review of World Energy June 2016. *Br. Pet.* **2016**, *201*.
2. Thakur, A.K.; Prabakaran, R.; Elkadeem, M.; Sharshir, S.W.; Arıcı, M.; Wang, C.; Zhao, W.; Hwang, J.Y.; Saidur, R. A state of art review and future viewpoint on advance cooling techniques for Lithium–ion battery system of electric vehicles. *J. Energy Storage* **2020**, *32*, 101771. [CrossRef]
3. Grigoratos, T.; Fontaras, G.; Giechaskiel, B.; Zacharof, N. Real world emissions performance of heavy-duty Euro VI diesel vehicles. *Atmos. Environ.* **2019**, *201*, 348–359. [CrossRef]
4. Chiasserini, C.F.; Rao, R.R. Energy efficient battery management. *IEEE J. Sel. Areas Commun.* **2001**, *19*, 1235–1245. [CrossRef]
5. Huber, C.; Kuhn, R. Thermal management of batteries for electric vehicles. In *Advances in Battery Technologies for Electric Vehicles*; Elsevier: Amsterdam, The Netherlands, 2015; pp. 327–358. [CrossRef].
6. Koltypin, M.; Aurbach, D.; Nazar, L.; Ellis, B. More on the performance of LiFePO4 electrodes—The effect of synthesis route, solution composition, aging, and temperature. *J. Power Sources* **2007**, *174*, 1241–1250. [CrossRef]
7. Doughty, D.H. Li Ion Battery Abuse Tolerance Testing-An Overview. 2006. Available online: https://www.osti.gov/servlets/purl/1725924 (accessed on 17 June 2021).
8. Zhang, S.; Xu, K.; Jow, T. The low temperature performance of Li-ion batteries. *J. Power Sources* **2003**, *115*, 137–140. [CrossRef]
9. Wang, Q.; Jiang, B.; Li, B.; Yan, Y. A critical review of thermal management models and solutions of lithium-ion batteries for the development of pure electric vehicles. *Renew. Sustain. Energy Rev.* **2016**, *64*, 106–128. [CrossRef]
10. Lin, H.P.; Chua, D.; Salomon, M.; Shiao, H.; Hendrickson, M.; Plichta, E.; Slane, S. Low-temperature behavior of Li-ion cells. *Electrochem. Solid State Lett.* **2001**, *4*, A71. [CrossRef]
11. Chowdhury, S.; Leitzel, L.; Zima, M.; Santacesaria, M.; Titov, G.; Lustbader, J.; Rugh, J.; Winkler, J.; Khawaja, A.; Govindarajalu, M. Total Thermal management of battery electric vehicles (BEVs). *SAE Tech. Pap. Ser.* **2018**, *1*. [CrossRef]
12. Meyer, J., Lustbader, J.A.; Rugh, J.P.; Titov, G.; Agathocleous, N.; Vespa, A. Range Extension Opportunities While Heating a Battery Electric Vehicle. 2018. Available online: https://doi.org/10.4271/2018-01-0066 (accessed on 17 June 2021).
13. Fuller, T.F.; Doyle, M.; Newman, J. Simulation and optimization of the dual lithium ion insertion cell. *J. Electrochem. Soc.* **1994**, *141*, 1. [CrossRef]
14. Doyle, M.; Newman, J.; Gozdz, A.S.; Schmutz, C.N.; Tarascon, J.M. Comparison of modeling predictions with experimental data from plastic lithium ion cells. *J. Electrochem. Soc.* **1996**, *143*, 1890. [CrossRef]
15. Feng, J.; He, Y.; Wang, G. Comparison study of equivalent circuit model of Li-Ion battery for electrical vehicles. *Res. J. Appl. Sci.* **2013**, *6*, 3756–3759. [CrossRef].
16. Wang, Z.; Ni, J.; Li, L.; Lu, J. Theoretical simulation and modeling of three-dimensional batteries. *Cell Rep. Phys. Sci.* **2020**, *1*, 100078. [CrossRef]
17. Basu, S.; Hariharan, K.S.; Kolake, S.M.; Song, T.; Sohn, D.K.; Yeo, T. Coupled electrochemical thermal modelling of a novel Li-ion battery pack thermal management system. *Appl. Energy* **2016**, *181*, 1–13. [CrossRef]
18. Saqli, K.; Bouchareb, H.; Naamane, A.; M'sirdi, N.; Oudghiri, M. Battery Pack Thermal Modeling, Simulation and electric model Identification. In Proceedings of the ICEERE2020 2nd International Conference on Electronic Engineering and Renewable Energy, Saidia, Morocco, 13–15 April 2020.

19. Zhu, L.; Xiong, F.; Chen, H.; Wei, D.; Li, G.; Ouyang, C. Thermal analysis and optimization of an EV battery pack for real applications. *Int. J. Heat Mass Transf.* **2020**, *163*, 120384. [CrossRef]
20. Deng, T.; Ran, Y.; Yin, Y.; Liu, P. Multi-objective optimization design of thermal management system for lithium-ion battery pack based on Non-dominated Sorting Genetic Algorithm II. *Appl. Therm. Eng.* **2020**, *164*, 114394. [CrossRef]
21. Jarrett, A.; Kim, I.Y. Influence of operating conditions on the optimum design of electric vehicle battery cooling plates. *J. Power Sources* **2014**, *245*, 644–655. [CrossRef]
22. Alhanouti, M.; Gießler, M.; Blank, T.; Gauterin, F. New electro-thermal battery pack model of an electric vehicle. *Energies* **2016**, *9*, 563. [CrossRef]
23. Bernardi, D.; Pawlikowski, E.; Newman, J. A general energy balance for battery systems. *J. Electrochem. Soc.* **1985**, *132*, 5. [CrossRef]
24. Gao, Z.; Chin, C.S.; Woo, W.L.; Jia, J. Integrated equivalent circuit and thermal model for simulation of temperature-dependent LiFePO4 battery in actual embedded application. *Energies* **2017**, *10*, 85. [CrossRef]
25. Gottapu, M.; Goh, T.; Kaushik, A.; Adiga, S.P.; Bharathraj, S.; Patil, R.S.; Kim, D.; Ryu, Y. Fully coupled simplified electrochemical and thermal model for series-parallel configured battery pack. *J. Energy Storage* **2021**, *36*, 102424. [CrossRef]
26. Shabani, B.; Biju, M. Theoretical modelling methods for thermal management of batteries. *Energies* **2015**, *8*, 10153–10177. [CrossRef]
27. Astaneh, M.; Andric, J.; Löfdahl, L.; Maggiolo, D.; Stopp, P.; Moghaddam, M.; Chapuis, M.; Ström, H. Calibration Optimization Methodology for Lithium-Ion Battery Pack Model for Electric Vehicles in Mining Applications. *Energies* **2020**, *13*, 3532. [CrossRef]
28. Kays W.M., Crawford M.E., Weigand B. *Convective Heat and Mass Transfer*, 4th ed.; McGraw-Hill Higher Education: Boston, MA, USA, 2005.
29. Ghiaasiaan, S.M. *Convective Heat and Mass Transfer*; CRC Press: Boca Raton, FL, USA, 2018.
30. Singer, S.; Nelder, J. Nelder-mead algorithm. *Scholarpedia* **2009**, *4*, 2928. [CrossRef]